Article:
Cao, L, Sun, Q and Magee, C (Cover date: December 2023) Reutilization of fluid flow pathways over 54 million years, offshore New Zealand. Basin Research, 35 (6). pp. 2349-2363. ISSN: 0950-091X

https://doi.org/10.1111/bre.12801

Reutilization of hydrothermal fluid flow pathways over 54 million years, offshore New Zealand

Liu Cao[1], Qiliang Sun[1,2*], Craig Magee[3]

[1]Key Laboratory of Tectonics and Petroleum Resources, China University of Geosciences (Wuhan), Ministry of Education, Wuhan 430074, China

[2]Laboratory for Marine Mineral Resources, Qingdao National Laboratory for Marine Science and Technology, Qingdao 266061, China

[3]Institute of Geophysics and Tectonics, School of Earth Science and Environment, University of Leeds, Leeds LS2 9JT, UK

Corresponding author: **Qiliang Sun** (sunqiliang@cug.edu.cn)

Abstract

Structures that facilitate fluid migration are common in sedimentary basins. We document several possible hydrothermal and/or volcanic vents located above a >157 km^2, late Cretaceous volcanic field in the Great South Basin, offshore New Zealand. Three of the four vents are vertically stacked, suggesting episodic re-use of the same fluid pathway between ~75 and ~56 Ma. A paleo-pockmark dated to ~49 Ma and free gas occurring within strata ~21 Myr old are located directly above these stacked vents. The spatial association of the vents, pockmark, and free gas further suggests re-use of the fluid migration pathway(s) extended for over 54 Myr. Our results imply that reutilization of fluid flow pathways can affect the distribution of fluids within basins over prolonged periods, potentially impacting hydrocarbon/geothermal exploration and geohazard assessment.

Keywords

Hydrothermal vent, fluid migration, gas chimney, pockmark, Great South Basin

1 Introduction

Focused fluid flow and associated fluid escape structures (e.g. hydrothermal vents, gas chimneys, mud diapirs, and pockmarks) commonly occur in sedimentary basins (e.g. Bischoff et al., 2019; Cartwright et al., 2007; Cartwright & Santamarina, 2015; Jackson et al., 2019; Jamtveit et al., 2004; Siregar et al., 2019; Svensen et al., 2004). Many sedimentary basins also host a variety of magmatic complexes (e.g. Jackson et al., 2013; Magee et al., 2014; Schofield et al., 2017; Song et al., 2017). In addition to feeding and creating volcanoes, this magmatism can also produce pockmarks and/or hydrothermal vents driven by magmatic volatile escape and intrusion-induced heating of pore fluids (e.g. Iyer et al., 2017; Mourgues et al., 2012; Svensen et al., 2006). Although these intrusion-related fluid escape structures form near-instantaneously (Planke et al., 2005), identification of vertically stacked hydrothermal vent systems suggests intrusions can direct fluid flow over millions of years (typically <10 Myr) (e.g. Roelofse et al., 2021). Similarly, the presence of fluid and gas indicators above some hydrothermal vents and volcanic edifices implies that their plumbing systems may be reactivated by and focus later fluid flow (e.g. hydrocarbon or carbon dioxide) long after magmatism has ceased (e.g. Holford et al., 2017; Manton et al., 2022; Roelofse et al., 2021; Sun et al., 2020a). Understanding the timeframes over which fluid escape structures can be re-used may help improve the exploration efficiency of associated fluid-related resources and aid de-risking of subsurface storage sites.

Here, we use 3D seismic reflection data from the Great South Basin, offshore New Zealand, to image and date a large central volcanic edifice, overlying volcanic and/or hydrothermal vents, and other fluid escape structures. The main volcanic edifice formed in the Late Cretaceous, above which three, vertically stacked volcanic and/or hydrothermal vents formed between ~75 Ma and ~56 Ma, seemingly sharing the same fluid migration pathway. In strata above these stacked vents are: (1) an erosional depression (a pockmark), which probably formed due to surficial fluid escape at ~49 Ma; and (2) a series of high-amplitude, negative-polarity reflections in shallower strata (~21 Myr old) that we suggest represent younger gas accumulations. Our analysis suggests that fluid escape structures and migration pathways were reutilized on multiple occasions over a prolonged time (~54 Myr), thereby influencing the distribution of fluids.

2 Geological Setting

Our study area is located within the Great South Basin (GSB), which is a rift basin located offshore the southern tip of the South Island of New Zealand (Fig. 1). The GSB covers an area of ~100,000 km^2 with present water depths of ~300 m to ~1000 m, and a maximum sedimentary sequence thickness of ~8.5 km (Evans, 1982; Killops et al., 1997). This rift basin formed during the Cretaceous breakup of Gondwana and comprises a series of graben and half-graben (Figs. 1a) (Cook et al., 1999).

The syn-rift Hoiho Group (Late Cretaceous) deposited along the axis of graben is mainly composed of terrestrial conglomerates, sandstones, shales, and coals (e.g., Killops et al., 1998; Mitchell et al., 2009) (Fig. 2). The Hoiho Group has been penetrated by several wells (e.g. the Tara-1 and Hoiho-1C) and is considered to be the principal hydrocarbon source rock in the GSB (Beggs et al., 1990). Post-rift strata marking a transition from a continental to marine environment were deposited between Late Cretaceous and Late Eocene, and can be sub-divided into the Pakaha Group (Late Cretaceous - Late Paleocene) and the Rakiura Group (Eocene) (Figs. 2-3) (Cook et al., 1999). The Pakaha Group is composed of the Kawau Formation (Late Cretaceous), Wickliffe Formation (Late Cretaceous - Late Paleocene), Taratu Formation (Late Cretaceous), and Tartan Formation (Late Paleocene - Paleocene) (Fig. 2). The Kawau Formation is mainly composed of transgressive sandstones and directly overlies the Hoiho Group and basement (Osli et al., 2018; Sahoo et al., 2022; Schiøler et al., 2010); the Kawau Formation is widely developed across the GSB and serves as the main reservoir and lateral migration pathway for fluids (Killops et al., 1997) (Fig. 2). The Wickliffe Formation is mainly composed of shale and clays (Chenrai, 2016; Meadows, 2009), whereas the Taratu Formation is mainly composed of organic-rich clays and thus forms one of the oil-prone formations in the basin (Osli et al., 2018; Shalaby et al., 2019). The Rakiura Group can be divided into the Laing Formation (clays) (Eocene) and the Tucker Cove Formation (marls) (Eocene) (Morley et al., 2017; Viskovic, 2010) (Fig. 2).

Intraplate igneous activity has occurred periodically across New Zealand, both onshore and offshore (e.g. Barrier et al., 2021; Field et al., 1989; Hoernle et al., 2006, 2020; Omosanya et al., 2021; Timm et al., 2009). Previous studies have divided the igneous activity across New Zealand into four stages that corresponded to different tectonic periods (e.g., Barrier et al., 2021; Bischoff et al., 2020). For example, syn-rift volcanism (105-83 Ma) associated with lithospheric thinning and rifting caused by the break-up of Gondwana is observed across the Canterbury Basin (e.g. the XXX) (Bischoff et al., 2020; Field et al., 1989; van der Meer et al., 2017). After rifting, the South Island of New Zealand entered a period of intense magmatic activity (83-66 Ma), caused by the separation of Zealandia from Australia and Antarctica (Barrier et al., 2021; Bischoff et al., 2020). Large volcanoes and volcanic fields formed during this period, such as the main edifice of Tuatara Volcanic Field (TVF) and associated sills and vents in the GSB (Phillips & Magee, 2020) and the Galleon Volcanics (GV) in the offshore Canterbury Basin (Fig. 1a) (Tulloch et al., 2009). Igneous activity at the Tuatara Volcanic Field continued periodically into the Early Eocene (to ~45 Ma), during post-rift tectonic quiescence (Omosanya et al., 2021; Phillips & Magee, 2020). Other monogenetic volcanic fields formed in the southwestern Pacific Plate (e.g. the Waiareka-Deborah in New Zealand) during the Cenozoic (60-30 Ma), which was defined as diffuse intraplate volcanism (Bischoff et al., 2020; Finn et al., 2005; Németh & Kereszturi, 2015; Scott et al., 2020). The Papatowai Volcanic Field (PVF) in the GSB was formed during this period and covered an area of >1600 km^2 (Bischoff et al., 2020) (Fig. 1). After the Miocene, intense magmatic activity occurred onshore and offshore New Zealand associated with the Hikurangi subduction zone and dextral strike-slip transgression along the Alpine Fault (Barrier et al., 2021; Bischoff et al., 2020; Omosanya et al., 2021; Nicol et al., 2007).

3 Data and Method

We use high-resolution, time-migrated 3D seismic reflection data (the Twahaki-Rigel 3D) from offshore the southern tip of the South Island of New Zealand (Fig. 1). The seismic survey covers an area of ~4880 km^2 and was acquired between late 2011 and early 2012, using eight 6 km long streamers. The data has a bin spacing of 6.25 × 37.5 m, a record length of 9.2 s, and a sampling interval of 2 ms (resampled to 4 ms in the final processed data). The seismic data is zero-phase processed and is displayed with the Society of Exploration Geophysicists (SEG) standard polarity, whereby a downward increase in acoustic impedance (a function of rock velocity and density) corresponds to a positive reflection event (red on seismic profiles) (Brown, 2011). Bertoni et al. (2019) report that the vertical resolution of the seismic data is ~10 m in the shallow subseafloor between ~1-2 s TWT, and is ~15-20 m between 2-3 s TWT.

We mapped nine regional stratigraphic boundaries/horizons: H2 (~21 Ma), T70 (~35 Ma), T60 (~42 Ma), T50 (~49 Ma), T10 (~56 Ma), H1 (~60 Ma), K100 (~66 Ma), K80 (~75 Ma), and K50

(~83 Ma) (Figs. 2-3). Horizon K50 represents the end of rifting, with horizons K100, T10, and T70 marking the tops of the Cretaceous, Paleocene, and Eocene successions, respectively. Mapped horizons, except for H1 and H2, were assigned an age based on previously reported biostratigraphic data from 14 offshore wells (Bertoni et al., 2018, 2019; Blanke, 2015; Hunt International Petroleum Co. NZ, 1977a, 1977b, 1977c, 1978a, 1978b, 1978c; Placid Oil Company, 1984a, 1984b; Sahoo et al., 2020, 2022; Schiøler & Raine, 2009; Schiøler et al., 2011, 2012, 2017) (Fig. 2). The ages of Horizon H1 and H2 were estimated from the strata thickness to the upper and lower adjacent horizons (e.g., T10, K100 and T70), with the assumption that the sedimentation rates were consistent.

To help characterize possible fluid escape structures (e.g. mounded structures), we extracted envelope and root mean square (RMS) attributes and variance slices from the 3D seismic volume. The envelope is the total instantaneous energy of the analytic signal (the complex trace), which is proportional to the reflection coefficient, and it is useful to identify discontinuities, lithologic variations, and faults (Alves et al., 2015; Subrahmanyam and Rao, 2008). The RMS is a seismic attribute that is commonly used to identify amplitude anomalies, whereas variance characterizes differences in adjacent traces so highlights amplitude anomalies and discontinuities (e.g. faults, igneous bodies, and channels) (Brown, 2011; Marfurt & Alves, 2014).

4 Results

4.1 Seismic characteristics of mounded structures

We observe a central edifice that comprises a series of stacked (up to 660 ms TWT thick), discontinuous, often strata-concordant, low-to-high amplitude reflections developed at K50 (Fig. 3). Beneath this central edifice, seismic reflections are poorly imaged and appear blanked, likely because overlying higher amplitude reflections have absorbed and/or scatted the seismic energy (Fig. 3); the basal surface of the central edifice thus cannot be confidently identified. The central edifice has a diameter of ~20 km and covers ~157 km^2 in the study area, although only part of the central edifice is imaged by our seismic data (Fig. 3). The top of the central edifice is marked by positive-polarity reflections and is onlapped by strata between horizons K50 and K80 (Fig. 3). Within the central edifice, conical-like structures are apparent that internally comprise have weak-to-chaotic seismic reflections (Fig. 3).

Four mounded structures are observed above the central edifice, within a vertical zone of chaotic and dim seismic imaging, and we name them M1 to M4 from the oldest to the youngest (Figs. 4-5, S1-S4). M1 appears to sit on top of the central edifice and Horizon K80 (~75 Ma), and has a diameter of ~1.6 km and area of ~2.01 km^2 (Figs. 3, 4, and 5a). It has a height of ~810 ms TWT. M2 is located ~2 km to the west of M1 (Figs. 3-4), and directly sits on top of Horizon K100 (~66

Ma; Fig. 5b). Among the four mounded structures, M2 has the largest diameter of ~3.8 km and covers an area of ~11.34 km^2. M2 has a maximum height of ~900 ms TWT. M3 is located directly on Horizon H1 (~60 Ma), and has a diameter of ~2.0 km, and an area of ~ 3.14 km^2 (Fig. 5c). M3 is ~250 ms TWT high. M4 sits on Horizon T10 (~56 Ma), 90 ms TWT above the summit of M1, and is the smallest and youngest mounded structure; it covers an area of ~1.77 km^2, and has a height of 140 ms TWT (Fig. 5d). M1, M3, and M4 are vertically stacked and although they occur within a vertical seismically chaotic zone (see details in the next section), they can be confidently identified from their conical shapes, sub-horizontal bases, and onlapping seismic reflections (Figs. 5-6, S1-S4). The tops of the mounded structures are usually characterized by weak, continuous, positive-polarity seismic reflections (M1, M3, and M4; Figs. 5a, 5c-5d). However, a strong, continuous, negative top is observed at M2 (Fig. 5b). The bases of mounded structures are flat or rugose, with positive-polarity seismic reflections. Interiors of mounded structures are characterized by chaotic seismic reflections (Fig. 5).

4.2 Depression and amplitude anomalies

A vertical chaotic zone, a sub-circular depression, and several high amplitude anomalies are observed in the study area above the mounded structures (Figs. 3, 4, and 6-7). The vertical chaotic zone is ~1.5 km wide and extends downward to Horizon T70, across the mounded structures, and to the central edifice (Fig. 6). A sub-circular depression with a diameter of 2.5 km and a depth of 200 ms TWT occurs at T50. This depression is situated ~300 ms TWT above M4 and it truncates underlying reflections (Figs. 6a-6c and 7). Strata within the depression onlap onto its side, and are characterized by high-amplitude seismic reflections (Figs. 6a-6b). Stacked high-amplitude, negative-polarity seismic anomalies occur at and around the top of the vertical chaotic zone between horizons T50 and T70 (Figs. 7-8). Some isolated high amplitude anomalies with diameters of 0.6-1.0 km also occur above Horizon T70 and can reach up to Horizon H2 (~21 Ma; Fig. 8). These amplitude anomalies are sub-circular in plan-view and, on average, have areas of ~0.4 km^2.

5 Discussion

5.1 Mounded structure origins

The stacked, discontinuous, positive polarity, often strata-concordant, low-to-high amplitude internal seismic reflections of the up to 660 ms TWT thick, >157 km^2 central edifice are similar to those of nearby volcanic complexes, such as the Tuatara Volcanic Field (Phillips & Magee, 2020) and the Papatowai Volcanic Field (Bischoff et al., 2020). Therefore, we interpret the central edifice as a volcanic field; the conical structures within the edifice are likely volcanic vents and the strata-concordant, high-amplitude reflections are probably eruptive products like lava flows (Fig. 3).

Based on seismic-stratigraphic onlap relationships, this volcanic field seemingly formed at K50 (83 Ma) and may have been active up to Horizon K80 (~75 Ma) (Fig. 3).

Seismic reflections onlapping onto the flanks of the mounded structures above the central edifice indicate that they formed at the free surface and were subsequently buried by sediment (Figs. 6c and 6f) (e.g. Hansen, 2006; Magee et al., 2021; Rateau et al., 2013; Smallwood & Maresh, 2002; Trude et al., 2003). No boreholes have penetrated M1-M4, and thus their ages cannot be directly dated. Yet by dating the age of onlapping and underlying reflections we can constrain the relative ages of the mounded structures, and thus suggest M1-M4 formed at ~75 Ma, ~66 Ma, ~60 Ma, and ~56 Ma, respectively (Fig. 5).

Mounded structures like M1-M4 are common in sedimentary basins and they have several possible origins, including carbonate buildup, mud volcanism, igneous volcanism, and hydrothermal venting (e.g., Burgess et al., 2013; Kirkham et al., 2018; Magee et al., 2013; Reynolds et al., 2017; Schofield & Totterdell, 2008). Carbonate buildups usually reflect the accumulation of organisms, such as reefs and algae, and in shallow-marine settings can have a mounded appearance (Heckel, 1974). However, although deep-water carbonate buildups have occasionally been reported, they do not form mounded structures with km-scale diameters and hundred m-scale heights (e.g., Vlahović et al., 2005). Given our study area was situated in a deep-water regime since ~75 Ma (Higgs et al., 2021; Killops et al, 1997; Osli et al., 2018; Shalaby et al., 2019), and the scale of the mounded structures mapped, we consider it unlikely that the mounded structures represent carbonate buildups.

Mud volcanoes usually occur above massive muddy deposits (Dimitrov, 2002; Mazzini & Etiope, 2017). Based on our interpretation, M1 likely sits on a volcanic field comprising stacked lavas and volcaniclastics, perhaps with some interbedded sedimentary strata (Phillips and Magee, 2020). The presence of predominantly igneous material beneath M1 and the thin stratal layers between the volcanic field and other mounded structures (especially M1 and M2), would likely limit the availability of mud, implying the mounded structures are probably not mud volcanoes (Figs. 3 and 6).

Igneous volcanoes mainly comprise crystalline lavas or volcaniclastic rocks that are typically denser and have higher seismic velocities than those of surrounding sedimentary rocks (e.g., Calvès et al., 2011). We thus expect buried igneous volcanoes to show high-amplitude, positive seismic reflections at their tops (cf., Magee et al., 2013; Reynolds et al., 2018; Sun et al., 2019; Zhao et al., 2016). Yet we observe moderate-to-weak seismic reflections across the tops of M1-M4, as well as the negative top of M2 (Figs. 5b and 6d), which seem inconsistent with an igneous volcano origin. However, we note that M1, M3, and M4 occur in a vertical chaotic zone where the seismic reflection data is dimmer than elsewhere, which may have muted the amplitude response of these mounded structures; i.e. we cannot rule out that they are volcanic vents. We also recognize that the negative polarity top of M2 could reflect the presence of an altered hyaloclastite layer blanketing the mound, whereby the alteration has reduced its density and seismic velocity to below that of the overlying Paleocene strata (Ellefsen et al., 2010). Alternatively, our mounded structures also appear similar to hydrothermal vents, which usually contain chaotic internal seismic reflections, have conical/crater/eye-like shapes, and weak-moderate tops (usually positive polarity), such as those documented in the offshore southern Australia (Jackson, 2012), the Møre Basin (Kjoberg et al., 2017; Planke et al., 2005) and the Qiongdongnan Basin (Wang et al., 2019). If M1, M3, and/or M4 are hydrothermal vents, their flat bases (Figs. 5b-5d) would suggest the fluids were probably released slowly from the subsurface into the overlying water column, and thus they did not eject shallow sediments to form a crater (Planke et al., 2005). Hydrothermal vents are often related to underlying magma intrusions (cf., Jackson, 2012; Planke et al., 2005). Although we observe no sills that directly connect to M1-M4, the presence of these vents above the volcanic field may suggest that magmatism, or at least the generation and migration of hydrothermal fluids within this area, occurred after the formation of main edifice in the volcanic field.

5.2 Reutilization of fluid escape structures

Because M1, M3, and M4 are vertically stacked and appear within the same vertical chaotic zone (Figs. 4, 6, and 9a), it seems reasonable to suggest that the younger vents may have reutilized the fluid feeder conduits of older vents; i.e. fluid flow was focused by pre-existing structures for ~17 Myrs. Roelofse et al (2021) similarly showed two stacked hydrothermal vents in the Modgunn Arch of the Norwegian Sea, formed at Late Cretaceous and Late Paleocenes, supporting our interpretation that hydrothermal fluid pathways can remain open for prolonged periods.

We observe that the vertical chaotic zone continues above M4 and is associated with stacked high-amplitude, negative polarity anomalies up to Horizon T70 (Fig. 6); together, these features resemble the typical seismic characteristics of gas chimneys and free gas (Cartwright & Santamarina, 2015; Gross et al., 2018; Løseth et al., 2011). In such systems, vertical chaotic zones like we observe are caused by the absorption of acoustic energy in overlying high-amplitude strata, which hinders the downward transmission of energy to the underlying fluid feeder system (Roy et al., 2016). Considering the gas accumulates within strata as young as Horizon H2 (~21 Ma), at least some gas-charging events were younger than ~21 Ma.

The depression observed within the gas chimney at Horizon T50 shows evidence of erosion as it truncates underlying reflections and contains reflections that onlap onto its sides (Figs. 7a-7b); these features suggest the depression formed at the contemporaneous seafloor at ~49 Ma, perhaps in response to fluid escape (c.f., Cartwright, 2007). We specifically interpret the depression as a pockmark because its bowl-like geometry, size, and seismic-stratigraphic relationship are similar to pockmarks observed elsewhere (Ho et al., 2018; Velayatham et al., 2018).

Because there are no borehole samples available from the interpreted ~49-21 Myr old gas chimney, pockmark, or free gas anomalies, we cannot ascertain the composition of the fluids involved in their formation, but we consider three possible origins: 1) hydrothermal fluids (e.g., CO_2) related to magmatic activity, perhaps similar to those that may have generated M1-M4 if they are hydrothermal vents (Niyazi et al., 2021; Sharma & Srivastava, 2014); 2) hydrocarbons generated from source rocks of the Hoiho Group (Killops et al., 1997; Omosanya & Harishidayat, 2019; Shalaby et al., 2019); or 3) a mixture of the above-mentioned two sources. With regards to hydrothermal activity, we note that there was a regional reduction in magmatic activity during tectonic quiescence between 66 Ma and 30 Ma (Bischoff et al., 2020). Such waning hydrothermal and magmatic activity may suggest the gas chimney and free gas anomalies, as well as the pockmark, did not form in response to hydrothermal fluid escape. Instead, it seems plausible that the fluid escape structures and free gas were produced by the release of hydrocarbons. We suggest that the porous sandstone of the Kawau Formation, which surrounded the volcanic field in the study area, and/or the fluid plumbing system of the hydrothermal vents M1, M3, and M4 may have provided a pathway for hydrocarbon migration from the deep-seated source rocks in the Hoiho Group (Figs. 7b and 9b). The migrating hydrocarbons may have temporarily accumulated around the peak of M4, because of its mounded morphology. When the overpressure exceeded the yield strength of overlying strata, the gas chimney (hydraulic fracturing) would have developed above M4. The explosive release of overpressured fluids through the gas chimney may have led to the disaggregation and expulsion of unconsolidated, shallow seabed sediments to form the observed pockmark (Figs. 7 and 9b). The widespread free gas anomalies, which extend upwards to Horizon H2 suggest that the gas chimney was active, either continuously or episodically, until at least to ~21 Ma (Horizon H2) (Fig. 9c).

Overall, our interpretation suggests that the M1, M3, and M4 vents and their plumbing system were utilized for fluid flow over 54 Myrs. The longevity of fluid flow pathways probably played important roles (providing hydrocarbon migration pathways) in linking the source rocks to the overlying reservoirs when the source rocks were deeply buried (mature), such as those in the Faroe-Shetland basins (Schofield et al., 2017) and the South China Sea (Sun et al., 2020a). Therefore, the longevity of fluid flow pathways may promote the accumulation of fluids (e.g. hydrocarbon). However, the longevity of fluid flow may also trigger seabed instability, when the transported fluids accumulate within the shallow strata or erupt onto the seabed. In general, reassessment of the hydrocarbon/geothermal exploration and geohazard assessment may be needed, where the longevity and reutilization of fluid flow pathways occur.

6 Conclusions

We examine a series of vertically stacked and connected fluid escape structures using high-resolution 3D seismic reflection data from the Great South Basin, offshore the South Island of New Zealand. Specifically, we recognize four hydrothermal and/or volcanic vents located above a huge ancient volcanic field formed in the Late Cretaceous. The hydrothermal and/orvolcanic vents formed periodically at ~75 Ma, ~66 Ma, ~60 Ma, and ~56 Ma, respectively. Fluid flow features including a gas chimney, a pockmark, and gas-charged strata are observed above these stacked vents and at least formed between ~49 Ma and ~21 Ma. The observed stacking of vents, a pockmark, and gas accumulations suggests that the fluid escape pathway was probably re-used multiple times over 54 Myr. This study indicates that reutilization of fluid flow pathways can control the distribution of fluids within basins over prolonged periods.

Acknowledgments

The authors thank the New Zealand Petroleum and Minerals for making the seismic reflection data used in this study publicly available. Deputy Editor Kerry Gallagher, and two reviewers, Dr. Hehe Chen and Dr. Nick Schofield are thanked for their constructive comments and suggestions that greatly improve this paper.

Open Research

3D seismic reflection data used in the study is available at the New Zealand Petroleum & Minerals Online Exploration Database (https://data.nzpam.govt.nz/GOLD/system/mainframe.asp).

References

Alves, T. M., Omosanya, K. d., & Gowling, P. (2015). Volume rendering of enigmatic high-amplitude anomalies in southeast Brazil: A workflow to distinguish lithologic features from fluid accumulations. *Interpretation, 3*(2), 1-14. http://doi.org/10.1190/INT-2014-0106.1

Bache, F., Sutherland, R., Stagpoole, V., Herzer, R., Collot, J., & Rouillard, P. (2012). Stratigraphy of the southern Norfolk Ridge and the Reinga Basin: A record of initiation of Tonga–Kermadec–Northland subduction in the southwest Pacific. *Earth and Planetary Science Letters*, *321-322*, 41-53. https://doi.org/10.1016/j.epsl.2011.12.041

Bache, F., Mortimer, N., Sutherland, R., Collot, J., Rouillard, P., Stagpoole, V., & Nicol, A. (2014). Seismic stratigraphic record of transition from Mesozoic subduction to continental breakup in the Zealandia sector of eastern Gondwana. *Gondwana Research*, *26*(3-4), 1060-1078. https://doi.org/10.1016/j.gr.2013.08.012

Barrier, A., Bischoff, A., Nicol, A., Browne, G. H., & Bassett, K. N. (2021). Relationships between volcanism and plate tectonics: A case-study from the Canterbury Basin, New Zealand. *Marine Geology*, *433*(433), 106397. https://doi.org/10.1016/j.margeo.2020.106397

Beggs, J. M., Challis, G. A., & Cook, R. A. (1990). Basement geology of the Campbell Plateau: Implications for correlation of the Campbell Magnetic Anomaly System. *New Zealand Journal of Geology and Geophysics*, *33*(3), 401-404. https://doi.org/10.1080/00288306.1990.10425696

Bertoni, C., Cartwright, J., Foschi, M., & Martin, J. (2018). Spectrum of gas migration phenomena across multilayered sealing sequences. *AAPG Bulletin*, *102*(6), 1011-1034. https://doi.org/10.1306/0810171622617210

Bertoni, C., Gan, Y., Paganoni, M., Mayer, J., Cartwright, J., Martin, J., van Rensbergen, P., Wunderlich, A., & Clare, A. (2019). Late Paleocene pipe swarm in the Great South – Canterbury Basin (New Zealand). *Marine and Petroleum Geology*, *107*, 451-466. https://doi.org/10.1016/j.marpetgeo.2019.05.039

Bischoff, A., Nicol, A., Barrier, A., & Wang, H. (2019). Paleogeography and volcanic morphology reconstruction of a buried monogenetic volcanic field (part 2). *Bulletin of Volcanology*, *81*(9), 57. https://doi.org/10.1007/s00445-019-1317-6

Bischoff, A., Barrier, A., Beggs, M., Nicol, A., Cole, J., & Sahoo, T. (2020). Volcanoes buried in Te Riu-a-Māui/Zealandia sedimentary basins. *New Zealand Journal of Geology and Geophysics*, *63*(4), 378-401. https://doi.org/10.1080/00288306.2020.1773510

Blanke, S. (2015). PEP 38264 Caravel ‐ 1 well completion report. In *New Zealand Petroleum Report* (PR4896).

Brown, A. R. (2011). *Interpretation of three-dimensional seismic data*, 7th ed., Society of Exploration Geophysicists and American Association of Petroleum Geologists, Tulsa, Okla.

Burgess, P. M., Winefield, P., Minzoni, M., & Elders, C. (2013). Methods for identification of isolated carbonate buildups from seismic reflection data. *AAPG Bulletin, 97*(7), 1071-1098. https://doi.org/10.1306/12051212011

Calvès, G., Schwab, A. M., Huuse, M., Clift, P. D., Gaina, C., Jolley, D., Tabrez, A. R., & Inam, A. (2011). Seismic volcanostratigraphy of the western Indian rifted margin: The pre-Deccan igneous province. *Journal of Geophysical Research: Solid Earth, 116*(B1). https://doi.org/10.1029/2010JB000862

Cartwright, J. (2007). The impact of 3D seismic data on the understanding of compaction, fluid flow and diagenesis in sedimentary basins. *Journal of the Geological Society, 164*(5), 881. http://doi.org/10.1144/0016-76492006-143

Cartwright, J., & Santamarina, C. (2015). Seismic characteristics of fluid escape pipes in sedimentary basins: Implications for pipe genesis. *Marine and Petroleum Geology*, *65*, 126-140. https://doi.org/10.1016/j.marpetgeo.2015.03.023

Chenrai, P. (2016). Seismic stratigraphy and fluid flow in the Taranaki and Great South Basins offshore New Zealand. The University of Manchester (United Kingdom).

Cook, R. A., Sutherland, R., & Zhu, H. (1999). *Cretaceous-Cenozoic Geology and Petroleum Systems of the Great South Basin, New Zealand*, Institute of Geological & Nuclear Sciences, Lower Hutt, New Zealand.

Dimitrov, L. I. (2002). Mud volcanoes—the most important pathway for degassing deeply buried sediments. *Earth-Science Reviews, 59*(1), 49-76. https://doi.org/10.1016/S0012-8252(02)00069-7

Eichhubl, P., Davatz, N. C., & Becker, S. P. (2009). Structural and diagenetic control of fluid migration and cementation along the Moab fault, Utah. *AAPG Bulletin, 93*(5), 653-681. https://doi.org/10.1306/02180908080

Ellefsen, M., Boldreel, L. O., & Larsen, M. (2010). Intra-basalt units and base of the volcanic succession east of the Faroe Islands exemplified by interpretation of offshore 3D seismic data. *Geological Society, London, Petroleum Geology Conference Series*, 7(1), 1033-1042. https://doi.org/10.1144/0071033

Evans, P. R. (1982). Petroleum potential of New Zealand. *Journal of Petroleum Geology*, *5*(1), 89-96. https://doi.org/10.1111/j.1747-5457.1982.tb00562.x

Field, B. D., Browne, G. H., Davy, B. W., & Survey, N. Z. G. (1989). *Cretaceous and Cenozoic Sedimentary Basins and Geological Evolution of the Canterbury Region, South Island, New Zealand*, New Zealand Geological Survey.

Gross, F., et al. (2018). Free gas distribution and basal shear zone development in a subaqueous landslide – Insight from 3D seismic imaging of the Tuaheni Landslide Complex, New Zealand. *Earth and Planetary Science Letters*, *502*, 231-243. https://doi.org/10.1016/j.epsl.2018.09.002

Hansen, D. M. (2006). The morphology of intrusion-related vent structures and their implications for constraining the timing of intrusive events along the NE Atlantic margin. *Journal of the Geological Society*, *163*(5), 789. https://doi.org/10.1144/0016-76492004-167

Hart, B. S., & Hamilton, T. S. (1993). High-resolution acoustic mapping of shallow gas in unconsolidated sediments beneath the strait of Georgia, British Columbia. *Geo-Marine Letters*, *13*(1), 49-55. http://doi.org/10.1007/BF01204392

Heckel, P. H. (1974). Carbonate Buildups in the Geologic Record: A Review, in *Reefs in Time and Space: Selected Examples from the Recent and Ancient*, edited by Laporte, L. F., p. 0, SEPM Society for Sedimentary Geology, http://doi.org/10.2110/pec.74.18.0090

Higgs, K. E., Funnell, R. H., & Browne, G. H. (2021). A multidisciplinary study of diagenesis and pore fluid evolution in frontier basins; an example from Canterbury and Great South basins, New Zealand. *Marine and Petroleum Geology*, *124*, 104817. https://doi.org/10.1016/j.marpetgeo.2020.104817

Ho, S., Imbert, P., Hovland, M., Wetzel, A., Blouet, J.-P., & Carruthers, D. (2018). Downslope-shifting pockmarks: interplay between hydrocarbon leakage, sedimentations, currents and slope's topography. *International Journal of Earth Sciences*, *107*(8), 2907-2929. https://doi.org/10.1007/s00531-018-1635-5

Hoernle, K., White, J. D. L., van den Bogaard, P., Hauff, F., Coombs, D. S., Werner, R., Timm, C., Garbe-Schönberg, D., Reay, A., & Cooper, A. F. (2006). Cenozoic intraplate volcanism on New Zealand: Upwelling induced by lithospheric removal. *Earth and Planetary Science Letters, 248*(1-2), 350-367. https://doi.org/10.1016/j.epsl.2006.06.001

Hoernle, K., Timm, C., Hauff, F., Tappenden, V., Werner, R., Jolis, E. M., Mortimer, N., Weaver, S., Riefstahl, F., & Gohl, K. (2020). Late Cretaceous (99-69 Ma) basaltic intraplate volcanism on and around Zealandia:

Tracing upper mantle geodynamics from Hikurangi Plateau collision to Gondwana breakup and beyond. *Earth and Planetary Science Letters*, *529*, 115864. https://doi.org/10.1016/j.epsl.2019.115864

Holford, S. P., Schofield, N., & Reynolds, P. (2017). Subsurface fluid flow focused by buried volcanoes in sedimentary basins: Evidence from 3D seismic data, Bass Basin, offshore southeastern Australia. *Interpretation*, *5*(3), SK39-SK50. https://doi.org/10.1190/INT-2016-0205.1

Hunt International Petroleum Co NZ. (1977a). Toroa-1 well completion report. In *New Zealand Petroleum Report*, PR691.

Hunt International Petroleum Co NZ. (1977b). Final report Kawau-1A. In *New Zealand Petroleum Report*, PR716.

Hunt International Petroleum Co NZ. (1977c). Pakaha-1 well completion report. In *New Zealand Petroleum Report*, PR703.

Hunt International Petroleum Co NZ. (1978a). Hoiho-1C well completion report. In *New Zealand Petroleum Report*, PR730.

Hunt International Petroleum Co NZ. (1978b). Tara-1 well completion report. In *New Zealand Petroleum Report*, PR732.

Hunt International Petroleum Co NZ. (1978c). Takapu-1 & Takapu-1A well completion report. In *New Zealand Petroleum Report*, PR733.

Iyer, K., Schmid, D. W., Planke, S., & Millett, J. (2017). Modelling hydrothermal venting in volcanic sedimentary basins: Impact on hydrocarbon maturation and paleoclimate. *Earth and Planetary Science Letters, 467*, 30-42. http://doi.org/10.1016/j.epsl.2017.03.023

Jackson, C. A. L., Schofield, N., & Golenkov. (2013). Geometry and controls on the development of igneous sill-related forced folds: A 2-D seismic reflection case study from offshore southern Australia. *GSA Bulletin, 125*(11-12), 1874-1890. https://doi.org/10.1130/B30833.1

Jackson, C. A. L. (2012). Seismic reflection imaging and controls on the preservation of ancient sill-fed magmatic vents. *Journal of the Geological Society, 169*(5), 503-506. https://doi.org/10.1144/0016-76492011-147

Jackson, C. A. L., Magee, C., & Hunt-Stewart, E. R. (2019). Cenozoic Contourites in the Eastern Great Australian Bight, Offshore Southern Australia: Implications For the Onset of the Leeuwin Current. *Journal of Sedimentary Research*, *89*(3), 199-206. https://doi.org/10.2110/jsr.2019.16

Jamtveit, B., Svensen, H., Podladchikov, Y. Y., & Planke, S. (2004). Hydrothermal vent complexes associated with sill intrusions in sedimentary basins. *Geological Society, London, Special Publications, 234*(1), 233. https://doi.org/10.1144/GSL.SP.2004.234.01.15

Killops, S. D., Cook, R. A., Sykes, R., & Boudou, J. P. (1997). Petroleum potential and oil‐source correlation in the Great South and Canterbury Basins. *New Zealand Journal of Geology and Geophysics*, *40*(4), 405-423. https://doi.org/10.1080/00288306.1997.9514773

Killops, S. D., Funnell, R. H., Suggate, R. P., Sykes, R., Peters, K. E., Walters, C., Woolhouse, A. D., Weston,

R. J., & Boudou, J. P. (1998). Predicting generation and expulsion of paraffinic oil from vitrinite-rich coals. *Organic Geochemistry*, *29*(1), 1-21. https://doi.org/10.1016/S0146-6380(98)00087-4

Kirkham, C., Cartwright, J., Hermanrud, C., & Jebsen, C. (2018). The genesis of mud volcano conduits through thick evaporite sequences. *Basin Research, 30*(2), 217-236. https://doi.org/10.1111/bre.12250

Kjoberg, S., et al. (2017). 3D structure and formation of hydrothermal vent complexes at the Paleocene-Eocene transition, the Møre Basin, mid-Norwegian margin. *Interpretation*, *5*(3), SK65-SK81. https://doi.org/10.1190/INT-2016-0159.1

Løseth, H., Wensaas, L., Arntsen, B., Hanken, N.-M., Basire, C., & Graue, K. (2011). 1000 m long gas blow-out pipes. *Marine and Petroleum Geology*, *28*(5), 1047-1060. https://doi.org/10.1016/j.marpetgeo.2010.10.001

Magee, C., Hunt-Stewart, E., & Jackson, C. A. L. (2013). Volcano growth mechanisms and the role of sub-volcanic intrusions: Insights from 2D seismic reflection data. *Earth and Planetary Science Letters*, *373*, 41-53. https://doi.org/10.1016/j.epsl.2013.04.041

Magee, C., Jackson, C. A. L., & Schofield, N. (2014). Diachronous sub-volcanic intrusion along deep-water margins: insights from the Irish Rockall Basin. *Basin Research, 26*(1), 85-105. https://doi.org/10.1111/bre.12044

Magee, C., Pichel, L. M., Madden‐Nadeau, A. L., Jackson, C. A. L., & Mohriak, W. (2021). Salt–magma interactions influence intrusion distribution and salt tectonics in the Santos Basin, offshore Brazil. *Basin Research*, *33*(3), 1820-1843. https://doi.org/10.1111/bre.12537

Manton, B., Müller, P., Mazzini, A., Zastrozhnov, D., Jerram, D.A., Millett, J.M., Schmid, D.W., Berndt, C., Myklebust, R., Planke, S., 2022. Characterizing ancient and modern hydrothermal venting systems. *Marine Geology, 447*, 106781. https://doi.org/10.1016/j.margeo.2022.106781

Marfurt, K. J., & Alves, T. M. (2014). Pitfalls and limitations in seismic attribute interpretation of tectonic features. *Interpretation*, *3*(1), SB5-SB15. https://doi.org/10.1190/INT-2014-0122.1

Mazzini, A., & Etiope, G. (2017). Mud volcanism: An updated review. *Earth-Science Reviews*, *168*, 81-112. https://doi.org/10.1016/j.earscirev.2017.03.001

Meadows, D. J. (2009). Stable isotope geochemistry of Paleocene to Early Eocene strata around southern New Zealand. Victoria University of Wellington.

Mitchell, M., Craw, D., Landis, C. A., & Frew, R. (2009). Stratigraphy, provenance, and diagenesis of the Cretaceous Horse Range Formation, east Otago, New Zealand. *New Zealand Journal of Geology and Geophysics*, *52*(3), 171-183. https://doi.org/10.1080/00288300909509884

Morley, C. K., Maczak, A., Rungprom, T., Ghosh, J., Cartwright, J. A., Bertoni, C., & Panpichityota, N. (2017). New style of honeycomb structures revealed on 3D seismic data indicate widespread diagenesis offshore Great South Basin, New Zealand. *Marine and Petroleum Geology*, *86*, 140-154. https://doi.org/10.1016/j.marpetgeo.2017.05.035

Mourgues, R., Bureau, D., Bodet, L., Gay, A., & Gressier, J. B. (2012). Formation of conical fractures in sedimentary basins: Experiments involving pore fluids and implications for sandstone intrusion mechanisms.

Earth and Planetary Science Letters, 313-314, 67-78. https://doi.org/10.1016/j.epsl.2011.10.029

Nader, F. H., Swennen, R., & Ellam, R. (2004). Reflux stratabound dolostone and hydrothermal volcanism-associated dolostone: a two-stage dolomitization model (Jurassic, Lebanon). *Sedimentology, 51*(2), 339-360. https://doi.org/10.1111/j.1365-3091.2004.00629.x

Németh, K., & Kereszturi, G. (2015). Monogenetic volcanism: personal views and discussion. *International Journal of Earth Sciences, 104*(8), 2131-2146. https://doi.org/10.1007/s00531-015-1243-6

Nicol, A., Mazengarb, C., Chanier, F., Rait, G., Uruski, C., & Wallace, L. (2007). Tectonic evolution of the active Hikurangi subduction margin, New Zealand, since the Oligocene. *Tectonics, 26*(4). https://doi.org/10.1029/2006TC002090

Niyazi, Y., Warne, M., & Ierodiaconou, D. (2021). Post-rift magmatism and hydrothermal activity in the central offshore Otway Basin and implications for igneous plumbing systems. *Marine Geology*, *438*, 106538. https://doi.org/10.1016/j.margeo.2021.106538

Omosanya, K. O., & Harishidayat, D. (2019). Seismic geomorphology of Cenozoic slope deposits and deltaic clinoforms in the Great South Basin (GSB) offshore New Zealand. *Geo-Marine Letters, 39*(1), 77-99. http://doi.org/10.1007/s00367-018-00558-8

Omosanya, K. O., Lawal, M. A., Iqbal, H. M., & Yizhaq, M. (2021). Massive seafloor mounds depict potential for seafloor mineral deposits in the Great South Basin (GSB) offshore New Zealand. *Scientific Reports*, *11*(1), 9185. https://doi.org/10.1038/s41598-021-88620-x

Osli, L. N., Shalaby, M. R., & Islam, M. A. (2018). Hydrocarbon generation modeling and source rock characterization of the Cretaceous–Paleocene Taratu Formation, Great South Basin, New Zealand. *Journal of Petroleum Exploration and Production Technology*, *9*(1), 125-139. https://doi.org/10.1007/s13202-018-0511-y

Phillips, T. B., & McCaffrey, K. J. W. (2019). Terrane Boundary Reactivation, Barriers to Lateral Fault Propagation and Reactivated Fabrics: Rifting Across the Median Batholith Zone, Great South Basin, New Zealand. *Tectonics*, *38*(11), 4027-4053. https://doi.org/10.1029/2019TC005772

Phillips, T. B., & Magee, C. (2020). Structural controls on the location, geometry and longevity of an intraplate volcanic system: the Tuatara Volcanic Field, Great South Basin, New Zealand. *Journal of the Geological Society*, *177*(5), 1039-1056. https://doi.org/10.1144/jgs2020-050

Placid Oil Company. (1984a). Well report, Rakiura - 1, Great South Basin, New Zealand. In *New Zealand Petroleum Report*, PR994.

Placid Oil Company. (1984b). Final geological well completion report, Pukaki - 1, Great South Basin, New Zealand, PPL38081. In *New Zealand Petroleum Report*, PR1005.

Planke, S., Rasmussen, T., Rey, S. S., & Myklebust, R. (2005). Seismic characteristics and distribution of volcanic intrusions and hydrothermal vent complexes in the Vøring and Møre basins. *Geological Society, London, Petroleum Geology Conference*, *6*(1), 833. https://doi.org/10.1144/0060833

Rateau, R., Schofield, N., & Smith, M. (2013). The potential role of igneous intrusions on hydrocarbon migration, West of Shetland. *Petroleum Geoscience*, *19*(3), 259-272. https://doi.org/10.1144/petgeo2012-035

Reynolds, P., Holford, S., Schofield, N., & Ross, A. (2017). The shallow depth emplacement of mafic intrusions on a magma-poor rifted margin: An example from the Bight Basin, southern Australia. *Marine and Petroleum Geology, 88*, 605-616. http://doi.org/10.1016/j.marpetgeo.2017.09.008

Reynolds, P., Schofield, N., Brown, R. J., & Holford, S. P. (2018). The architecture of submarine monogenetic volcanoes - insights from 3D seismic data. *Basin Research*, *30*, 437-451. https://doi.org/10.1111/bre.12230

Roelofse, C., Alves, T. M., & Omosanya, K. d. O. (2021). Reutilisation of hydrothermal vent complexes for focused fluid flow on continental margins (Modgunn Arch, Norwegian Sea). Basin *Research, 33*(2), 1111-1134. https://doi.org/10.1111/bre.12507

Roy, S., Hovland, M., & Braathen, A. (2016). Evidence of fluid seepage in Grønfjorden, Spitsbergen: Implications from an integrated acoustic study of seafloor morphology, marine sediments and tectonics. *Marine Geology*, *380*, 67-78. https://doi.org/10.1016/j.margeo.2016.07.002

Sahoo, T. R., Strogen, D. P., Browne, G. H., & Nicol, A. (2022). Evolution of syn- to early post-rift facies in rift basins: insights from the Cretaceous–Paleocene of the Great South Basin, New Zealand. *Basin Research, 34*(3), 1113-1142. https://doi.org/10.1111/bre.12652

Schofield, A., Holford, S., Millett, J., Brown, D., Jolley, D., Passey, S. R., Muirhead, D., Grove, C., Magee, C., Murray, J., Hole, M., Jackson, C. A. -L., & Stevenson, C., 2017. Regional magma plumbing and emplacement mechanisms of the Faroe-Shetland Sill Complex: implications for magma transport and petroleum systems within sedimentary basins. *Basin Research, 29*, 41-63. https://doi.org/10.1111/bre.12164.

Schofield, A., Totterdell, J., 2008. *Distribution, Timing and Origin of Magmatism in the Bight and Eucla Basins*, p. 19. Geoscience Australia Record 2008/24.

Schiøler, P., Rogers, K., Sykes, R., Hollis, C. J., Ilg, B., Meadows, D., Roncaglia, L., & Uruski, C. (2010). Palynofacies, organic geochemistry and depositional environment of the Tartan Formation (Late Paleocene), a potential source rock in the Great South Basin, *New Zealand. Marine and Petroleum Geology, 27*(2), 351-369. https://doi.org/10.1016/j.marpetgeo.2009.09.006

Schiøler, P., & Raine, J. I. (2009). Palynology of lower Hoiho Group in the Great South Basin and Clipper and Horse Range Formations in the Canterbury Basin, GNS Science Consultancy Report, 2009/361. In *New Zealand Petroleum Report* (PR4348, pp. 1–67).

Schiøler, P., Raine, J. I., Crundwell, M. P., Griffin, A., Hollis, C. J., Kulhanek, D. K., et al. (2011). Revised biostratigraphy and well correlation, Canterbury Basin, New Zealand, GNS Science Consultancy Report 2011/12. In *New Zealand Petroleum Report* (PR4365, pp. 1–142).

Schiøler, P., Raine, J. I., Crundwell,M. P., Fohrmann,M., Griffin, A., Hollis, C. J., et al. (2012). Revised biostratigraphy and well correlation, Canterbury Basin, New Zealand; updated with results from Cutter-1 well. GNS Science Consultancy Report, 2012/248, 164 p. in *New Zealand Petroleum Report*, PR4621.

Schiøler, P., Browne, G. H., Cameron, H., King, P. R., Strogen, D. P., Sahoo, T., & Funnell, R. H. (2017). Great South Basin: National wells audit pilot project play analysis report, GNS Science Consultancy Report 2017/20. In *New Zealand Petroleum Report* (PR5428, pp. 1–70).

Scott, J. M., Pontesilli, A., Brenna, M., White, J. D. L., Giacalone, E., Palin, J. M., & le Roux, P. J. (2020). The Dunedin Volcanic Group and a revised model for Zealandia's alkaline intraplate volcanism. *New Zealand Journal of Geology and Geophysics, 63*(4), http://doi.org/510-529. 10.1080/00288306.2019.1707695

Shalaby, M. R., Osli, L. N., Kalaitzidis, S., & Islam, M. A. (2019). Thermal maturity and depositional palaeoenvironments of the Cretaceous-Palaeocene source rock Taratu Formation, Great South Basin, New Zealand. *Journal of Petroleum Science and Engineering*, *181*, 106156. https://doi.org/10.1016/j.petrol.2019.06.020

Sharma, R., & Srivastava, P. K. (2014). *Hydrothermal Fluids of Magmatic Origin, in Modelling of Magmatic and Allied Processes*. Edited by Kumar, S. & Singh, R. N. 181-208, Springer International Publishing, Cham. https://doi.org/10.1007/978-3-319-06471-0_9

Siregar, E., Omosanya, K. O., Magee, C., & Johansen, S. E. (2019). Impacts of fault-sill interactions on sill emplacement in the Vøring Basin, Norwegian North Sea. *Journal of Structural Geology*, *126*, 156-174. https://doi.org/10.1016/j.jsg.2019.06.006

Smallwood, J. R., & Maresh, J. (2002). The properties, morphology and distribution of igneous sills: modelling, borehole data and 3D seismic from the Faroe-Shetland area. *Geological Society, London, Special Publications*, *197*(1), 271-306. https://doi.org/10.1144/GSL.SP.2002.197.01.11

Song, X., Li, C., Yao, Y., & Shi, H. (2017). Magmatism in the evolution of the South China Sea: Geophysical characterization. *Marine Geology, 394*, 4-15. https://doi.org/10.1016/j.margeo.2017.07.021

Subrahmanyam, D., & Rao, P. (2008). *Seismic attributes-A review*. paper presented at 7th international conference & exposition on petroleum geophysics, Hyderabad, India.

Sun, Q., Jackson, C. A. L., Magee, C., & Xie, X. (2019). Deeply buried ancient volcanoes control hydrocarbon migration in the South China Sea. *Basin Research*, *32*(1), 146-162. https://doi.org/10.1111/bre.12372

Sun, Q., Alves, T. M., Zhao, M., Sibuet, J.-C., Calvès, G., & Xie, X. (2020a). Post-rift magmatism on the northern South China Sea margin. *GSA Bulletin*, *132*(11-12), 2382-2396. https://doi.org/10.1130/B35471.1

Sun, Q., Magee, C., Jackson, C. A. L., Mitchell, S. J., & Xie, X. (2020b). How do deep-water volcanoes grow? *Earth and Planetary Science Letters, 542*, 116320. https://doi.org/10.1016/j.epsl.2020.116320

Sutherland, R., et al. (2010). Lithosphere delamination with foundering of lower crust and mantle caused permanent subsidence of New Caledonia Trough and transient uplift of Lord Howe Rise during Eocene and Oligocene initiation of Tonga-Kermadec subduction, western Pacific. *Tectonics, 29*(2). https://doi.org/10.1029/2009TC002476

Svensen, H., Planke, S., Malthe-Sørenssen, A., Jamtveit, B., Myklebust, R., Rasmussen Eidem, T., & Rey, S. S. (2004). Release of methane from a volcanic basin as a mechanism for initial Eocene global warming. *Nature, 429*(6991), 542-545. https://doi.org/10.1038/nature02566

Svensen, H., Jamtveit, B., Planke, S., & Chevallier, L. (2006). Structure and evolution of hydrothermal vent complexes in the Karoo Basin, South Africa. *Journal of the Geological Society, 163*(4), 671-682. https://doi.org/10.1144/1144-764905-037

Timm, C., Hoernle, K., Van Den Bogaard, P., Bindeman, I., & Weaver, S. (2009). Geochemical Evolution of Intraplate Volcanism at Banks Peninsula, New Zealand: Interaction Between Asthenospheric and Lithospheric Melts. *Journal of Petrology*, *50*(6), 989-1023. https://doi.org/10.1093/petrology/egp029

Tóth, Z., Spiess, V., & Jensen, J. (2014a). Seismo-acoustic signatures of shallow free gas in the Bornholm Basin, Baltic Sea. *Continental Shelf Research, 88*, 228-239. https://doi.org/10.1016/j.csr.2014.08.007

Tóth, Z., Spiess, V., Mogollón, J. M., & Jensen, J. B. (2014b). Estimating the free gas content in Baltic Sea sediments using compressional wave velocity from marine seismic data. *Journal of Geophysical Research: Solid Earth, 119*(12), 8577-8593. https://doi.org/10.1002/2014JB010989

Trude, J., Cartwright, J., Davies, R. J., & Smallwood, J. (2003). New technique for dating igneous sills. *Geology*, *31*(9), 813-816. https://doi.org/10.1130/G19559.1

Tulloch, A. J., Ramezani, J., Mortimer, N., Mortensen, J., van den Bogaard, P., & Maas, R. (2009). Cretaceous felsic volcanism in New Zealand and Lord Howe Rise (Zealandia) as a precursor to final Gondwana break-up. *Geological Society, London, Special Publications*, *321*(1), 89-118. https://doi.org/10.1144/SP321.5

van der Meer, Q. H. A., Waight, T. E., Whitehouse, M. J., & Andersen, T. (2017). Age and petrogenetic constraints on the lower glassy ignimbrite of the Mount Somers Volcanic Group, New Zealand. *New Zealand Journal of Geology and Geophysics*, *60*(3), 209-219. https://doi.org/10.1080/00288306.2017.1307232

Velayatham, T., Holford, S. P., & Bunch, M. A. (2018). Ancient fluid flow recorded by remarkably long, buried pockmark trains observed in 3D seismic data, Exmouth Plateau, Northern Carnarvon Basin. *Marine and Petroleum Geology*, *95*, 303-313. https://doi.org/10.1016/j.marpetgeo.2018.05.007

Viskovic, G. P. D. (2010). Investigation of Fluid Migration Pathways in the Shallow Subsurface of the Great South Basin, through the use of High- Resolution Seimic Imaging of Fault and Fracture Systems. MSC thesis. University of Otago.

Vlahović, I., Tišljar, J., Velić, I., & Matičec, D. (2005). Evolution of the Adriatic Carbonate Platform: Palaeogeography, main events and depositional dynamics. *Palaeogeography, Palaeoclimatology, Palaeoecology*, *220*(3), 333-360. https://doi.org/10.1016/j.palaeo.2005.01.011

Wang, L., Sun, Z., Yang, J., Sun, Z., Zhu, J., Zhuo, H., & Stock, J. (2019). Seismic characteristics and evolution of post-rift igneous complexes and hydrothermal vents in the Lingshui sag (Qiongdongnan basin), northwestern South China Sea. *Marine Geology*, *418*, 106043. https://doi.org/10.1016/j.margeo.2019.106043

Zhao, F., Alves, T. M., Wu, S., Li, W., Huuse, M., Mi, L., Sun, Q., & Ma, B. (2016). Prolonged post-rift magmatism on highly extended crust of divergent continental margins (Baiyun Sag, South China Sea). *Earth and Planetary Science Letters*, *445*, 79-91. https://doi.org/10.1016/j.epsl.2016.04.001

Figure Captions

Figure 1. (a) Locations of the Great South Basin (GSB) and the study area (modified from the New Zealand Petroleum and Minerals, 2014). The central edifice (CE; red dashed line), the Tuatara volcanic field (TVF; Phillips & Magee, 2020) and the Papatowai volcanic field (PVF; Bischoff et al., 2020) are marked with; (b) Time-structure map of Horizon T50 (~49 Ma). Locations of mounded structures (M1 - M4) and figures used in this study are labelled.

Figure 2. Schematic diagram of the Great South Basin (modified from Killops et al., 1997; Cook et al., 1999; Meadows, 2009). The horizons and locations of wells with radiometric ages are from Bertoni et al. (2019), Sahoo et al. (2022) and Schiøler et al. (2010), respectively. MA: magmatic activities; SDMA: Subduction-related magmatic activities; DIMA: Diffuse intraplate magmatic activities; PRMA: Post-rift magmatic activities; SRMA: Syn-rift magmatic activities.

Figure 3. Seismic profile (a) and its interpretation (b). Seismic horizons and main features including the central edifice (CE), mounded structures (M1, M2, M3 and M4), a vertical chaotic zone (VCZ), a depression (D1) and high-amplitude seismic anomalies (AAs) in the study area are labelled. See location in Figure 1.

Figure 4. 3D map showing the central edifice (CE), mounded structures (M1-M4), vertical chaotic zone (VCZ) and depression (D1) to display their spatial relationship. Mounded structures M1, 3 and 4 are vertically stacked.

Figure 5. (a), (b), (c) and (d) Seismic profiles showing the characteristics of mounded structures (M1, M2, M3 and M4). Onlapping seismic reflections could be identified on the flanks of these mounded structures; (e), (f), (g) and (h) amplitudes envelope of mounded structures; (i), (j), (k) and (l) showing the 3-D shapes of mounded structures. The white dashed lines are the locations of seismic profiles shown in (a)-(h).

Figure 6. Seismic profiles (a and d), amplitude envelopes (b and e) and their associated interpretation (c and f) showing the characteristics of mounded structures (M1, M2, M3 and M4), a vertical chaotic zone (VCZ), a depression (D1) and high-amplitude anomalies (AAs). The mounded structures present as conical bodies in the amplitude envelops, and onlapping seismic reflections are observed at their flanks.

Figure 7. Seismic characteristic of the depression (D1) in the study area. (a) and (b) Seismic profiles crossing through the depression. Sediments within the depression onlap onto its flanks; (c) 3-D morphology of the depression; (d) Coherence slice of 2040 ms (TWT: two-way travel time).

Figure 8. (a) Seismic profile shown the characteristics of depression (D1) and high-amplitude anomalies (AAs); (b-d) RMS amplitude attributes extracted along the blue dashed line (T70), black dashed line and cyan dashed line (H2) in (a). Seismic amplitude anomalies (AAs) show as high values (warm color).

Figure 9. Evolution model of the hydrothermal vents and focused fluid flow system in the study area. (a)-(c) Formation of hydrothermal vents M1 (~75 Ma), M2 (~66 Ma) and M3 (~60 Ma) above the volcanic field; (d) Formation of hydrothermal vent M4 (~56 Ma). M1, M3 and M4 shared the same hydrothermal fluid pathway; (e) Fluids firstly accumulated at the peak of hydrothermal vent (M4) and then escaped onto the paleo-seabed to form the pockmark (D1) through the vertical fluid migration pathway (VCZ) in the Early Eocene (~49 Ma); (f) Fluids continued to migrate upward and charged into the strata as young as ~21 Ma (Horizon H2).

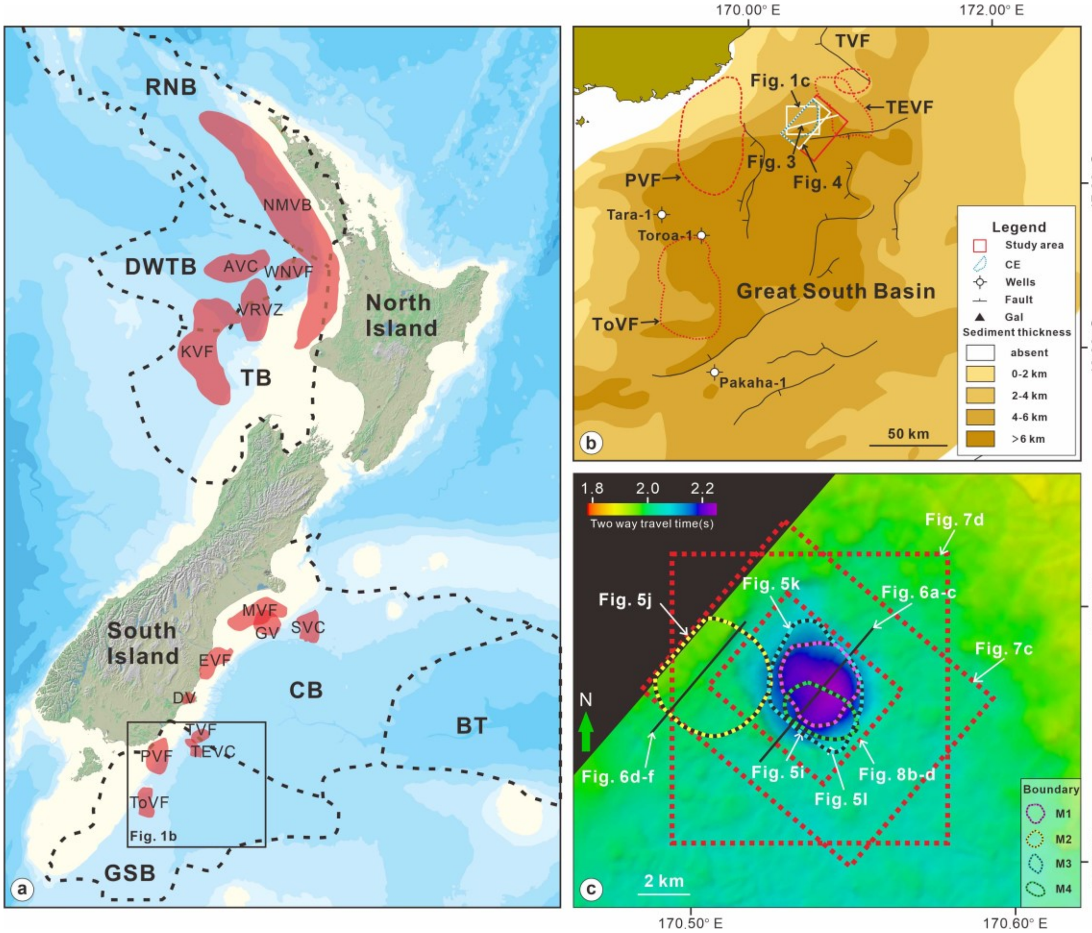

Figure 1. (**a**) Map showing the region bathymetry of New Zealand and location of offshore volcanoes; (**b**) Locations of the Great South Basin (GSB) and the study area (modified from the New Zealand Petroleum and Minerals, 2014); (**c**) Time-structure map of Horizon T50 (~49 Ma). Locations of the central edifice (CE; red dashed line), mounded structures (M1 - M4) and figures used in this study are labelled. RNB: Reinga Northland Basin (XX Ma); DWTB: Deep-water Taranaki Basin; TB: Taranaki Basin; GSB: Great South Basin; CB: Canterbury Basin; BT: Bounty Trough; NWVB: Northland-Mohakatino volcanic belts; AVC: Aotea volcanic complex; WNVF: West Ngatutura volcanic filed; VRVZ: Vulcan-Rommey volcanic belts; KVF: Kaiwero volcanic field; MVF: Maahunui volcanic field; GV: Galleon Volcanics; SVC: Sloop volcanic field; EVF: East Waiareka-Deborah volcanic field; DV: Dunedin volcano; TVF: the Tuatara volcanic field; TEVF: Tapuku East volcanic complex; PVF: the Papatowai volcanic field; ToVF: Toroa volcanic field. (Bischoff et al., 2020; Phillips&Magee, 2020; Tulloch et al., 2009).

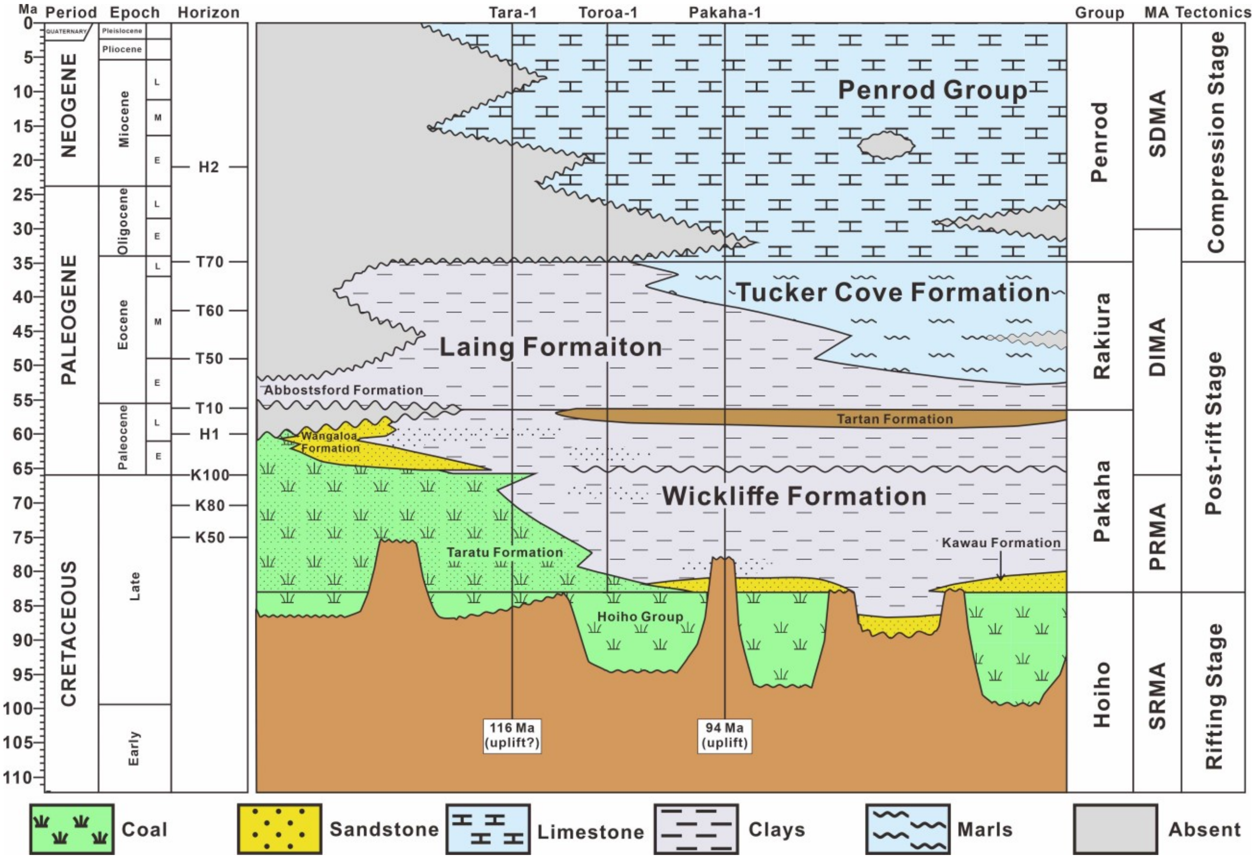

Figure 2. Schematic diagram of the Great South Basin (modified from Killops et al., 1997; Cook et al., 1999; Meadows, 2009). The horizons and locations of wells with radiometric ages are from Bertoni et al. (2019), Sahoo et al. (2022), Schiøler et al. (2010), respectively. MA: magmatic activities; SDMA: Subduction-related magmatic activities; DIMA: Diffuse intraplate magmatic activities; PRMA: Post-rift magmatic activities; SRMA: Syn-rift magmatic activities.

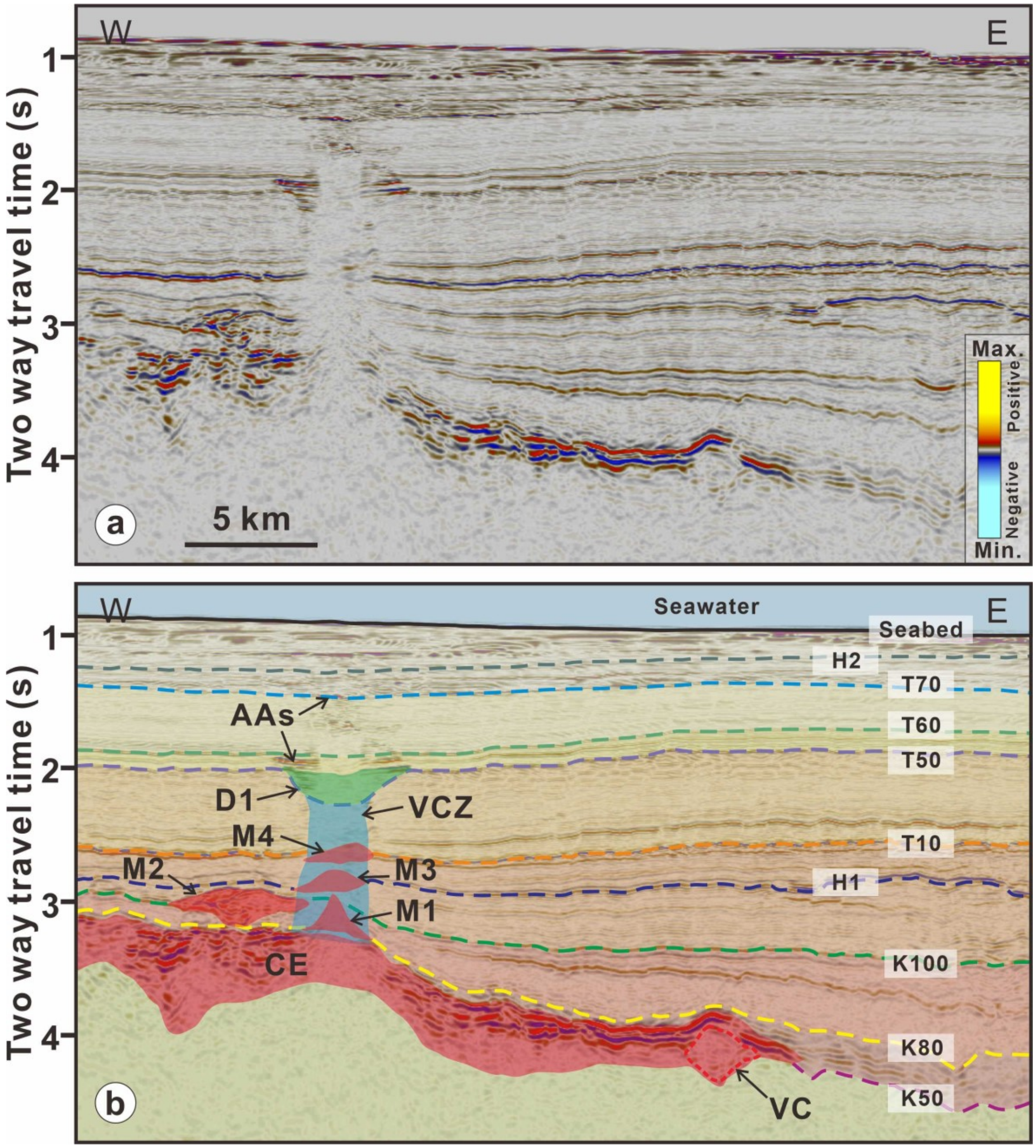

Figure 3. Seismic profile (**a**) and its interpretation (**b**). Seismic horizons and main features including the central edifice (CE), volcanic cone (VC), mounded structures (M1, M2, M3 and M4), a vertical chaotic zone (VCZ), a depression (D1) and high amplitude anomalies (AAs) in the study area are labelled. See location in Figure 1.

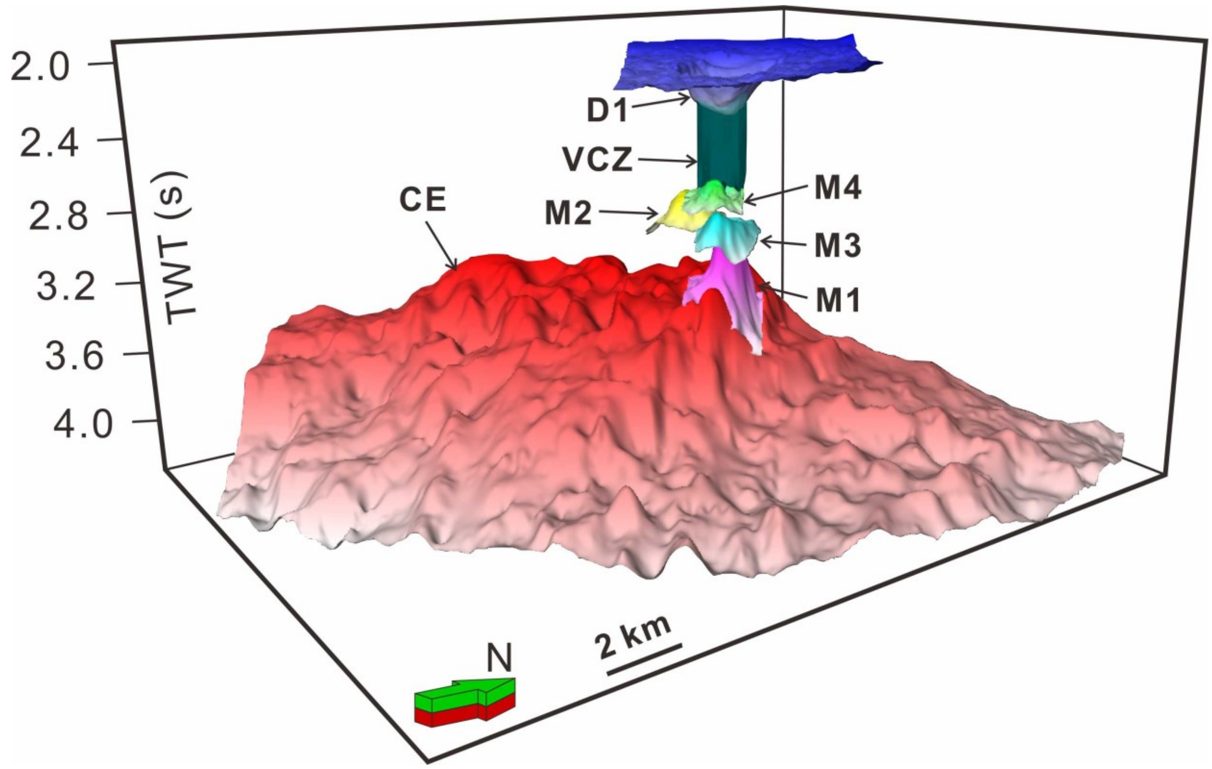

Figure 4. 3D map showing the central edifice (CE) in the study area, mounded structures (M1-M4), vertical chaotic zone (VCZ) and depression (D1) to display their spatial relationship. Mounded structures M1, 3and 4 are vertically stacked.

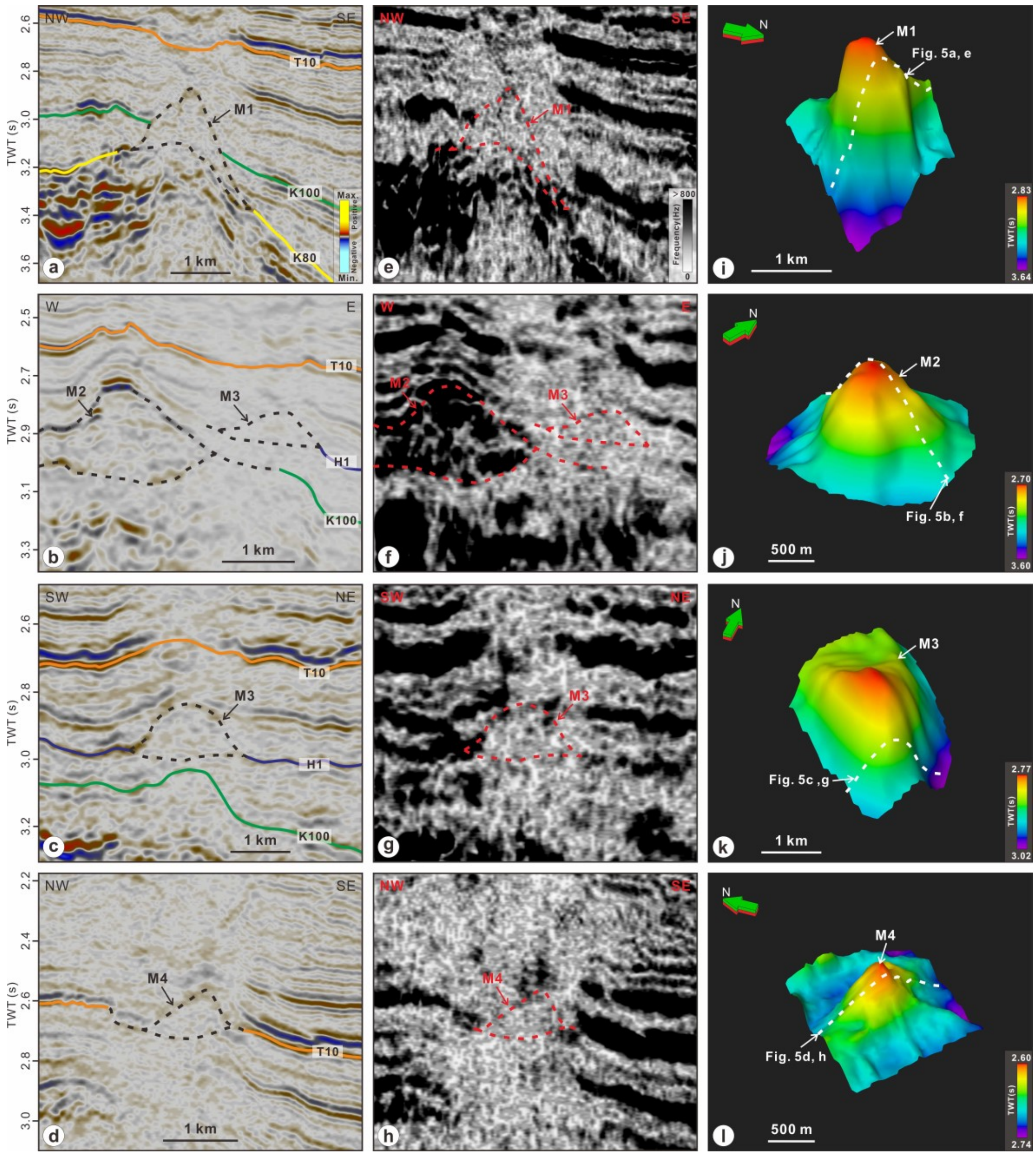

Figure 5. (**a**), (**b**), (**c**) and (**d**) Seismic sections showing the characteristics of mounded structures (M1, 2, 3 and 4). Onlapping seismic reflections could be identified on the flanks of these mounded structures. (**e**), (**f**), (**g**) and (**h**) Amplitudes envelope of mounded structures; (**i**), (**j**), (**k**) and (**l**) Showing the 3-D shapes of mounded structures. The white dashed lines are the locations of seismic sections shown on (a)-(h).

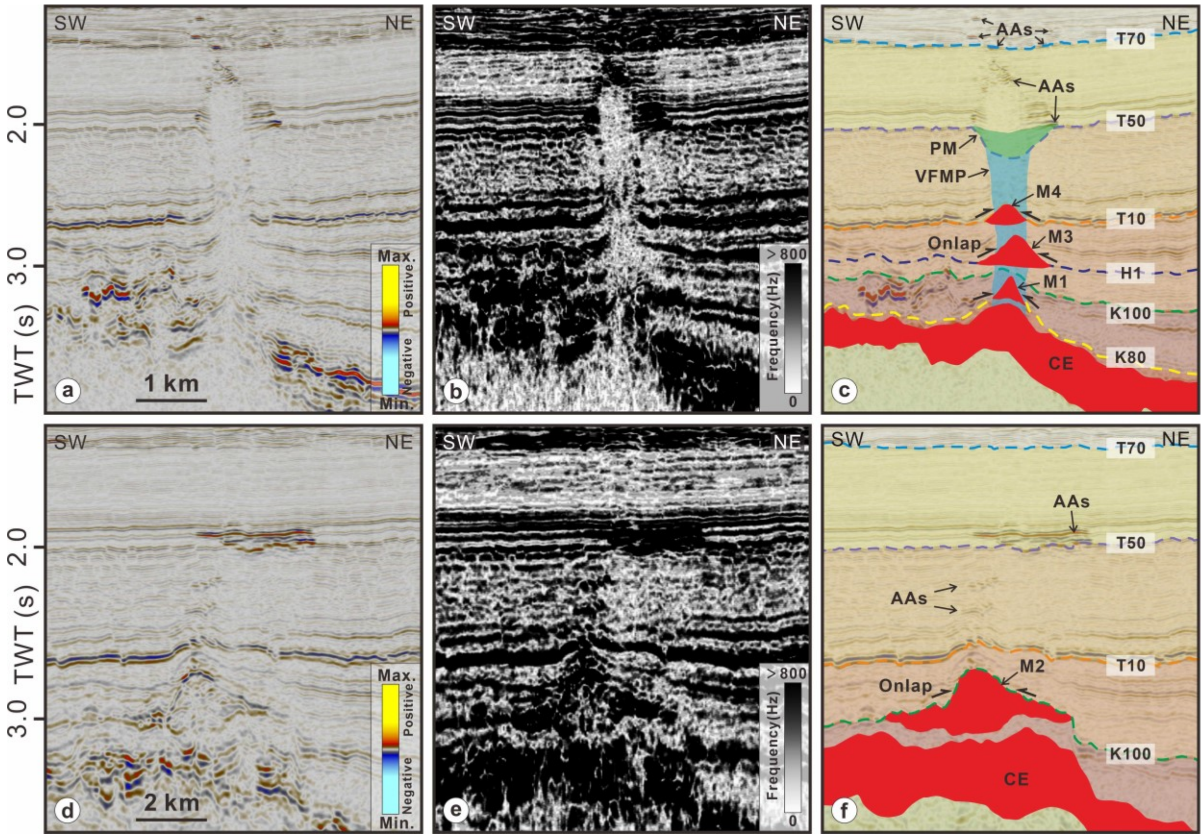

Figure 6. Seismic profiles (**a** and **d**), amplitude envelopes (**b** and **e**) and their associated interpretation (**c** and **f**) showing the characteristics of mounded structures (M1, M2, M3 and M4), a vertical chaotic zone (VCZ), a depression (D1) and high amplitude anomalies (AAs). The mounded structures present as conical bodies in the amplitude envelops, and onlapping seismic reflections are observed at their flanks.

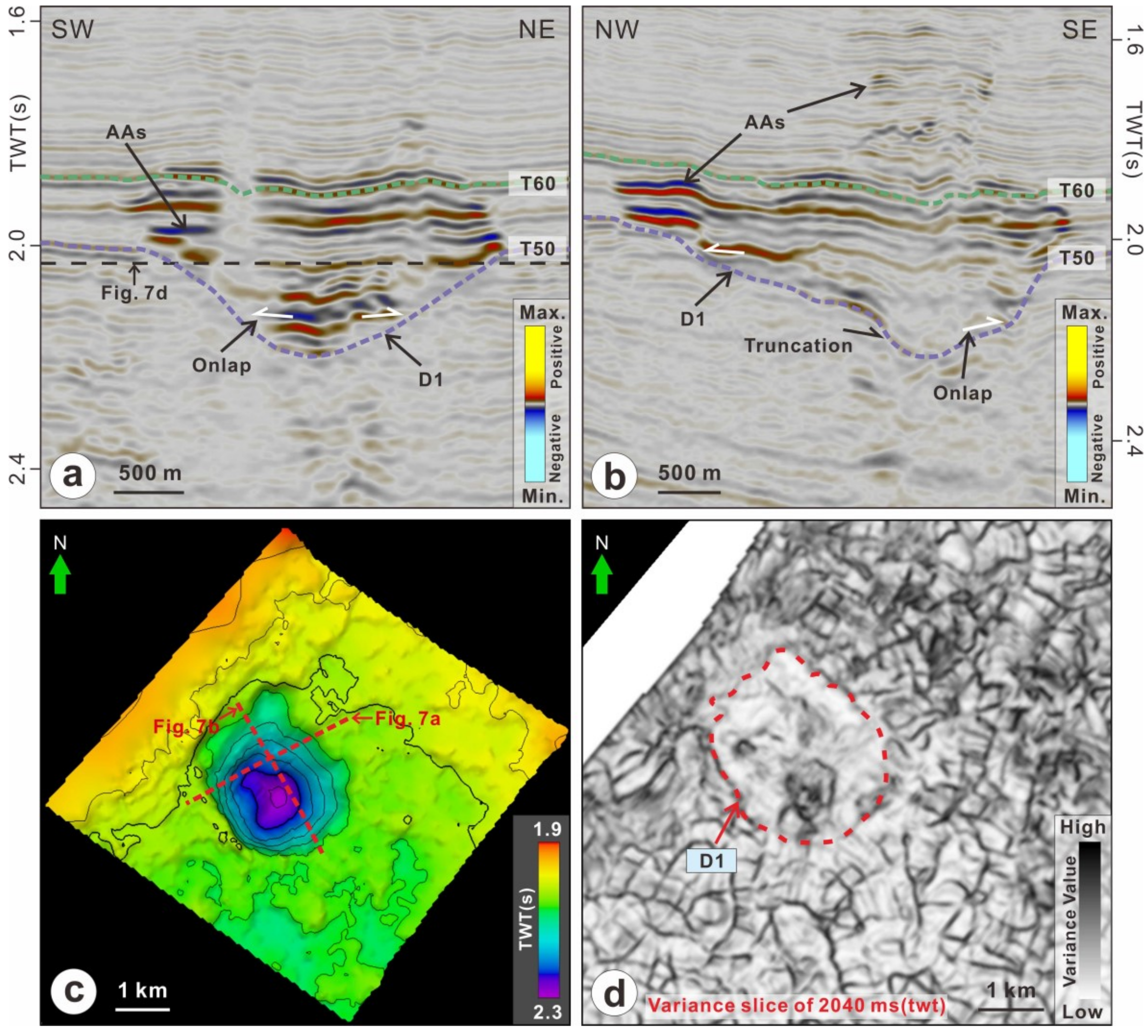

Figure 7. Seismic characteristic of the depression (D1) in the study area. (**a**) and (**b**) Seismic profiles crossing through the depression. Sediments within the depression onlapped onto its boundaries; (**c**) 3-D morphology of the depression; (**d**) Coherence slices of 2040 ms (twt).

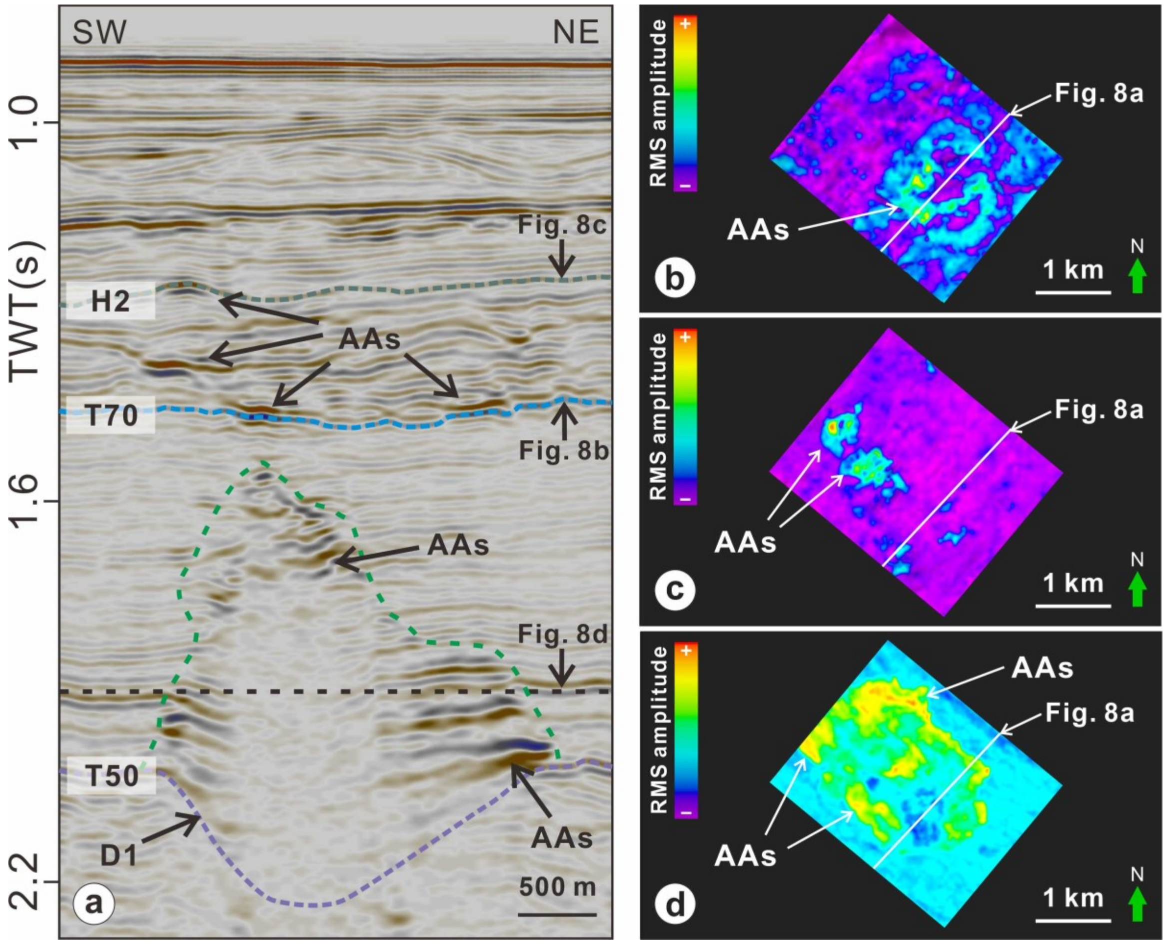

Figure 8. (**a**) Seismic profile shown the characteristics of depression (D1) and high amplitude anomalies (AAs). (**b-d**) RMS amplitude attribute extracted along the blue dashed line (T70), black dashed line and cyan dashed line (H2). Seismic amplitude anomalies (AAs) show as high values (warm color)

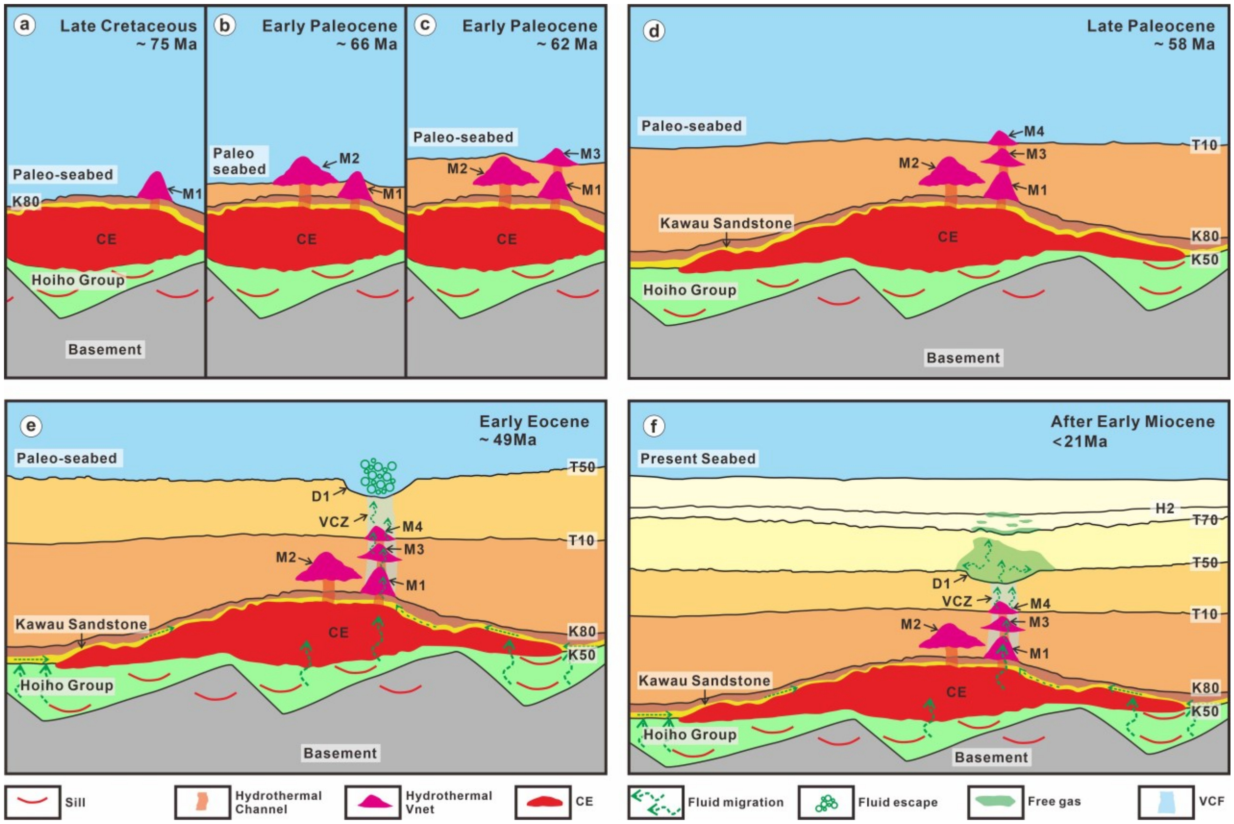

Figure 9. Evolution model of the hydrothermal vents and focused fluid flow system in the study area. (a)-(c) Formation of hydrothermal vents M1 (~75 Ma), M2 (~66 Ma) and M3 (~60 Ma) above the volcanic field; (d) Formation of hydrothermal vent M4 (~56 Ma). M1, M3 and M4 shared the same hydrothermal fluid pathways; (e) Fluids firstly accumulated at the peak of hydrothermal vent (M4) and then escaped onto the paleo-seabed to form the pockmark (D1) through the vertical fluid migration pathway (VCZ) in the Early Eocene (~49 Ma); (f) Fluids continued to migrate upward and charge strata as young as those of Horizon H2 (~21 Ma)